fibers

MDPI

Article

Investigation of Mechanical Properties and Morphology of Multi-Walled Carbon Nanotubes Reinforced Cellulose Acetate Fibers

Quazi Nahida Sultana [1], Md Mahmudul Hasan [1], Sakib Iqbal [1], Ishraq Shabib [2], Aniruddha Mitra [1] and Mujibur Khan [1,*]

[1] Department of Mechanical Engineering, Georgia Southern University, Statesboro, GA 30460, USA; qn00123@georgiasouthern.edu (Q.N.S.); mh10134@georgiasouthern.edu (M.M.H.); si00423@georgiasouthern.edu (S.I.); mitra@georgiasouthern.edu (A.M.)

[2] School of Engineering & Technology, Central Michigan University, Mt. Pleasant, MI 48859, USA; shabi1i@cmich.edu

* Correspondence: mkhan@georgiasouthern.edu; Tel.: +912-478-8004

Academic Editor: Yulin Deng
Received: 30 August 2017; Accepted: 6 November 2017; Published: 10 November 2017

Abstract: Cellulose acetate (CA) fibers were reinforced with multi-walled carbon nanotubes (MWCNTs) at 0.5%, 1.0%, 1.5% and 2.0%. Yield strength, ultimate tensile strength, fracture strain and toughness of the nanocomposite fiber increased up to 1.5 wt. % of the carbon nanotube (CNT) loading, however, further inclusion (2.0%) of MWCNTs in CA decreased the mechanical properties. Experimental properties were also compared with analytical predictions using a Shear lag model for strength and the rule of mixture for modulus. A solution spinning process, coupled with sonication, mixing, and extrusion, was used to process the CNT-reinforced composite fiber. Scanning electron microscopy (SEM) images of the cross sections of neat CA and CA-MWCNT fibers showed the formation of voids and irregular features. The enhanced interconnected fibrillation in the CNT-reinforced CA samples resulted in improved mechanical properties, which were observed by tensile testing. Fourier transform infrared spectroscopy (FTIR) spectra showed the area under the curve for C–H bonding after the inclusion of CNT. There was no significant shift of wavenumber for the inclusion of MWCNT in the CA matrix, which indicates that the sonication process of the CNT-loaded solution did not degrade the CA bonding structure.

Keywords: tensile properties; multi-walled carbon nanotube; cellulose acetate; fibrils structure; Fourier transform infrared spectroscopy

1. Introduction

All synthetic polymers are made from fossil sources and play a very important role in our daily life. However, the supply of fossil sources is decreasing day by day. The disposal of plastic waste from synthetic polymers is increasing which causes environmental pollution [1]. The environmental impacts include the massive rise in sea levels, increases in carbon dioxide, extreme weather conditions and widespread extinction of animals and plants. So, new materials for the same purpose should be produced from sustainable, ecological and eco-efficient industries and green chemical sources [2].

Cellulose is a naturally abundant polymer sourced from trees and a derivative of this is cellulose acetate (CA), which is one of the most important, widely used organic esters. CA can be utilized in many fields, including composite materials, textiles, sensors and for electromagnetic protection. If it is carbon nanotube (CNT) reinforced, the superior mechanical and electrical properties of the composite fiber are useful in the design of light weight space or combat dress. Body monitoring

sensors can also be implemented with this technology. Hybrid composites in, woven material or clothing can be used for electromagnetic shielding due to the capability of CNTs to absorb microwave frequency. There are many potential fields where CNT-reinforced CA fibers and their derivatives will be useful. CNT-strengthened hybrid composites can be used to make wind turbine and water craft hulls and are considered to replace synthetic polymers with natural biodegradable polymer, for many applications. CA is prepared through a chemical reaction of cellulose and acetic anhydride. Acetic acid is used as a solvent while sulfuric acid performs as a catalyst [3,4]. Cotton, crops, horticulture, and wood are the primary sources of cellulose polymer [5,6]. Nevertheless, a strong intermolecular hydrogen bonding network in natural cellulose creates a multitude of process challenges in creating fiber, whereas processing fiber from cellulose-based derivatives, such as CA is easier because of the solubility of CA in conventional organic solvent [7,8] which is most commonly used in dry and wet spinning processes. Additionally, CA has other appealing qualities, for example, its hydrophilic conduct, biocompatibility, and biodegradability [4], which make it a reasonable applicant material for use in biocomposites. CA is also a very cheap polymer compared to other polymeric sources and it is very hard, has good impact resistance, appealing texture, etc. [9].

CNTs have outstanding electrical, mechanical, and thermal properties [10,11]. For this reason, it is a promising material for biological and biomedical applications, textiles, coating film, nanosensors, etc. [12,13]. Young's modulus and [14] the tensile strength of CNTs are exceptionally high [15]. CNTs have been used [10,16–23] as reinforcing agents to produce nanocomposite polymers and fibers. Researchers have tried to come up with hybrid fiber systems by combining these fibers to obtain the high strength and stiffness of CNT.

Also in order to utilize these properties, CNTs should be aligned to preferred directions in the polymer matrix materials. All of these endeavors are made with the infusion of single or multi-walled CNTs.

CNT orientation, especially along the fiber axis is an exceptionally critical part in producing high elastic properties in CNT-based polymeric nanocomposite fibers [24]. The CNT filler and polymer matrix interface play the most important part in the load transfer mechanism. The characteristics of these interfaces will directly govern the composite material strength and stiffness. Specific surface area is highest in the case of rod-shaped filler CNT compared to any other shape of filler particle. Hence rod-shaped filler in CA fiber will help more in load transfer when properly orientated [25–27]. Melt spinning and solution spinning are the standard processing methods used for high volume production of nanocomposite fiber. CNTs can be dispersed into the solvent system and the preferred CNT orientation within fibers is achievable during the drawing step of the solution spinning process. Researchers have investigated the effect of an aqueous environment with different pH on cellulose and cellulose-based Kraft pulp with fourier transform infrared spectroscopy (FTIR) [28].

In our experiment, fabrication of both neat CA and CA fibers loaded with MWCNTs at a loading level of 0.5–2.0 wt. % was achieved by a solution spinning process. Mechanical test responses of CNT-reinforced CA polymer nanocomposite fibers were studied in this experiment. The morphology of the fibers was studied using SEM and FTIR.

2. Experimental Details

Multi-walled carbon nanotubes (MWCNTs) were dispersed into a binary solvent system of acetone and dimethylacetamide (DMAc) at 70 wt. % and 30 wt. %, respectively, then CA powder was added slowly to the solvent. Using a Sonics VCX130 horn sonicator (Sonics and Materials Inc., Newtown, CT, USA), the MWCNT particles were dispersed for 45 min at 30% amplitude. The beaker was placed in a water bath and an ice pack to avoid the heat. Then, 25 wt. % of CA was added slowly into the CNT dispersed solvents and the solution was stirred by an overhead stirrer for 3–4 h at 40 °C to get a homogenous mixture. The mixture was fed into the hopper and extruded through an extruder attached to a lab scale spinning line as shown in Figure 1. There were three zones (hopper (40 °C), L-shaped channel (35 °C) and extruder (35 °C)) in the spinning line. Filaments were continuously extruded under constant tension and precipitated after contacted with water. The fibers were collected using

a take-up roll and then washed with iso-propyl alcohol (IPA) and deionized water (DI) to remove solvents completely, Residual solvents and water content were removed by placing the fibers in a vacuum chamber at 1 Pa pressure and 25 °C for 2 h. All ingredients were procured from Sigma Aldrich Inc. (St. Louis, MO, USA) and Cheaptubes Inc. (Cambridgeport, VT, USA). Afterwards, the single fiber was characterized by SEM, FTIR, and a tensile testing machine.

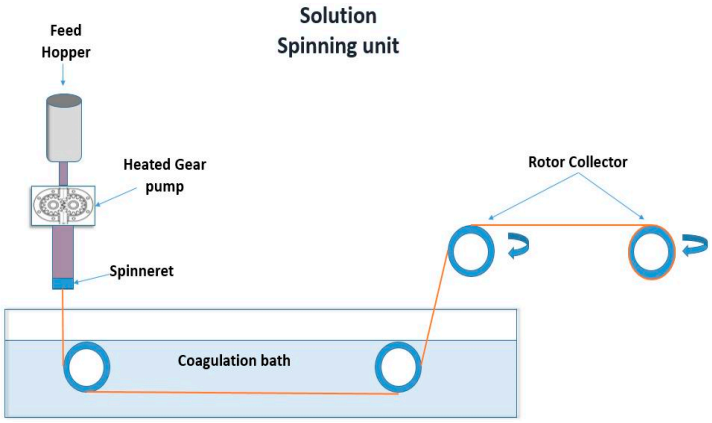

Figure 1. Laboratory solution spinning line.

A Shimadzu EZ-LX fiber testing machine (Shimadzu Corporation, Suzhou, Jiangsu, China) with a 20-N load cell was used for tensile tests in accordance with ASTM D3379-75 standards for individual filaments from each category. The diameter of the filaments was measured using an optical microscope (Hirox KH-7700) (Hirox-USA, Inc., Hackensack, NJ, USA) as seen in Figure 2. Three measurements of the diameter were taken longitudinally along a 30 mm length for each regular filament. Then, the average value of the three diameters was used for the stress calculation. Tensile tests were performed at a crosshead speed of 2.5 mm/min with a gauge length of 30 mm. Table 1 shows the tensile test data while Figures 3 and 4 represent the bar charts of the tensile test data and representative stress-strain diagrams, respectively, for five categories of fibers.

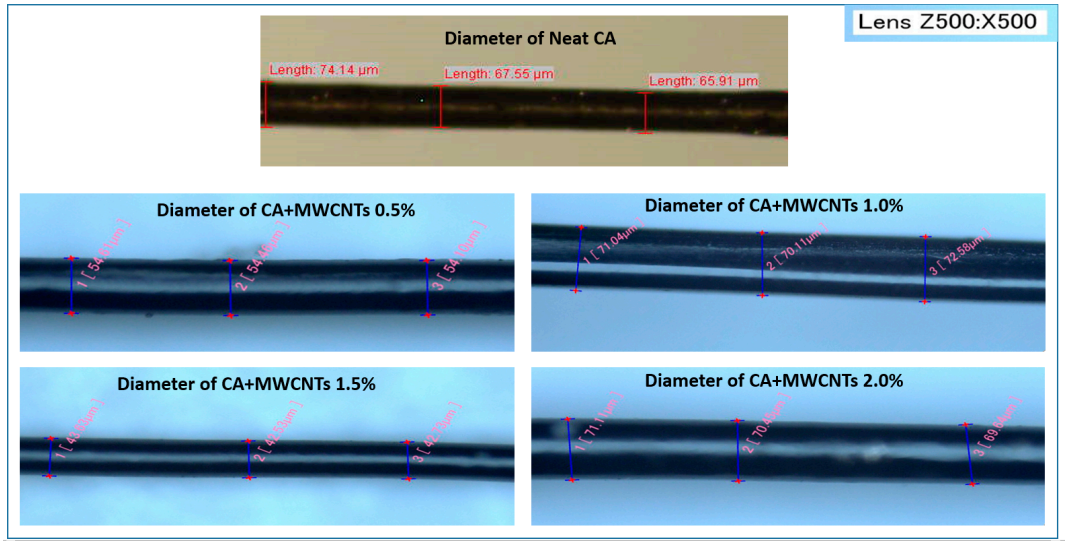

Figure 2. Optical microscopic images of fiber diameter.

Scanning electron microscopy (SEM) analyses were performed by a JEOL JSM-7600F scanning electron microscope (JEOL USA Inc. Peabody, MA, USA) for both CA and CA-MWCNT nanocomposite

fibers. To observe and image the surface and the cross section, the fibers were cut using fine scissors and mounted on a cylindrical stub by double-sided tape, vertically and horizontally. Then the samples were sputtered and coated with a layer of gold to improve surface conductivity.

The FTIR spectra of the CA and CA-MWCNTs was obtained in the range of 600–4000 cm^{-1} using a Thermo Nicolet Avatar 370 Fourier-transformer (FTIR) instrument (LabX, Midland, ON, Canada). Fiber filaments were placed across the diamond crystal using a high-pressure clamp, the fiber was pressed to the crystal surface and then a background spectrum was collected. The background spectrum contains the information about the molecules of gases and solvents. To get the information for the sample, the background spectrum is subtracted from the sample spectrum. All spectra were collected at 4 cm^{-1} spectral resolution and 100 scans were added. The KnowItAll TM software was used to analyze all spectra.

Table 1. Tensile test results.

Type	Parameters	Fiber Diameter (mm)	Yield Strength (MPa)	Modulus (GPa)	Ultimate Strength (MPa)	Fracture Strain (%)	Modulus of Toughness (MJ/m^3)
Neat Cellulose Acetate	Average	0.065	59.00	1.41	73.28	22.20	9.72
	Standard deviation	0.010	8.9	0.59	10.3	7.5	2.7
Cellulose Acetate + MWCNT 0.5%	Average	0.059	79.25	1.79	106.85	25.93	20.40
	Standard deviation	0.02	4.7	0.82	9.4	9.1	6.6
Cellulose Acetate + MWCNT 1.0%	Average	0.075	82.25	1.81	110.0	29.94	25.12
	Standard deviation	0.02	13.9	0.68	15.9	10.9	6.6
Cellulose Acetate + MWCNT 1.5%	Average	0.042	97.50	1.97	133.29	37.20	33.50
	Standard deviation	0.01	15.5	0.57	31	7.9	18.3
Cellulose Acetate + MWCNT 2.0%	Average	0.096	63.25	1.56	86.70	32.58	24.45
	Standard deviation	0.005	8.4	0.11	14.6	5.2	3.7

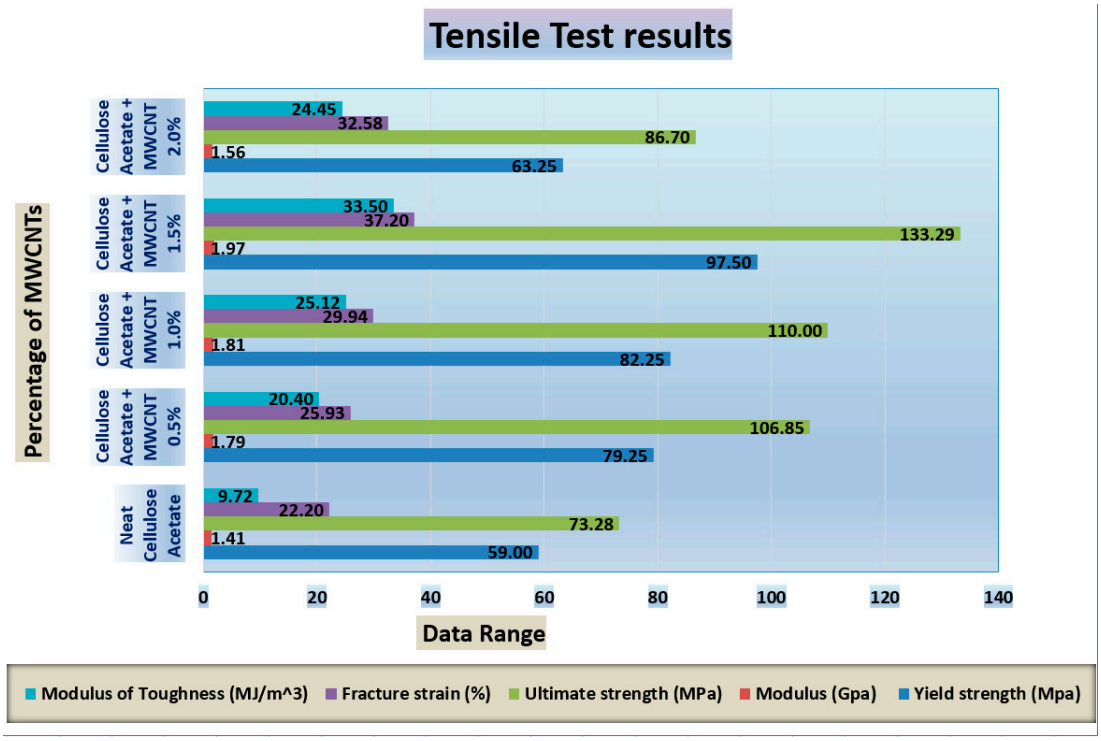

Figure 3. Representative tensile test results bar chart of (**a**) neat cellulose acetate (CA) (**b**) 0.5% cellulose acetate-multi-walled carbon nanotube (CA-MWCNT) (**c**) 1.0% CA-MWCNT (**d**) 1.5% CA-MWCNT (**e**) 2.0% CA-MWCNT.

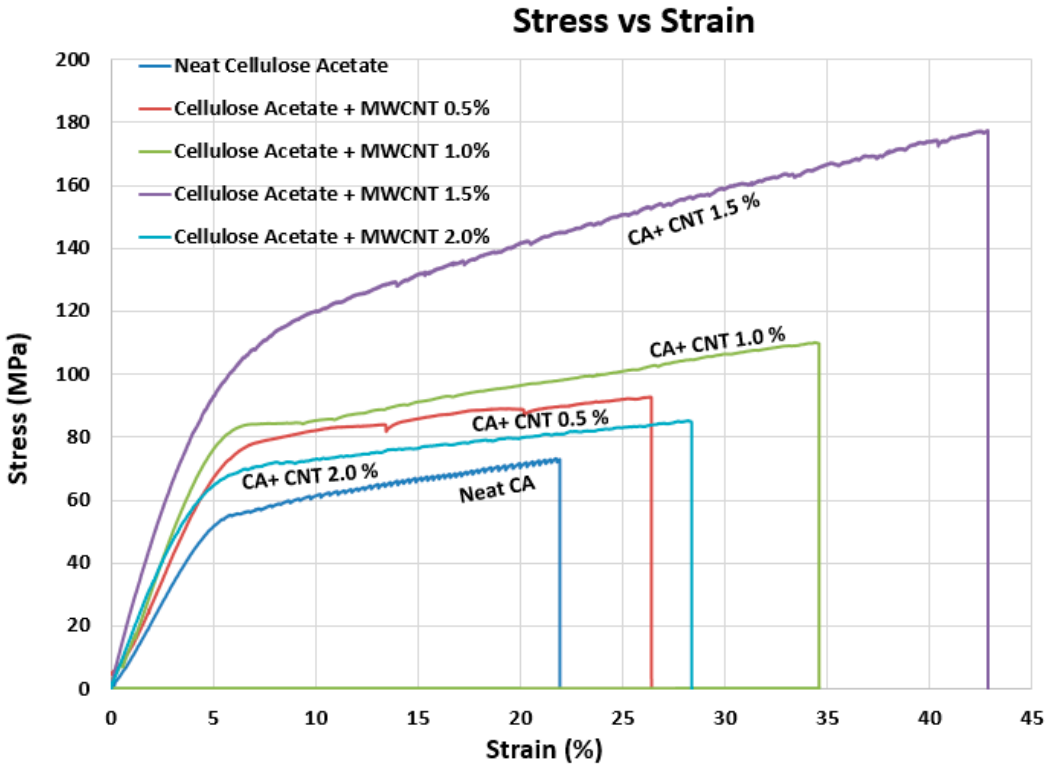

Figure 4. Representative stress-strain curves (**a**) neat CA (**b**) 0.5% CA-MWCNT (**c**) 1.0% CA-MWCNT (**d**) 1.5% CA-MWCNT (**e**) 2.0% CA-MWCNT.

3. Theoretical Prediction

Theoretical strength and modulus of CA reinforced with CNTs are calculated in this section. Micromechanical theories were used to calculate and verify the upper and lower bounds of the modulus.

3.1. Upper and Lower Bounds of Modulus

Micromechanical theories based on the minimum complementary energy and rules of mixture are used extensively for the theoretical bounds of composite materials. The uniaxial test for modulus with normal stresses [29] can be shown as,

$$\frac{1}{E_e^-} \leq \frac{1-C}{E_p} + \frac{C}{E_i} \tag{1}$$

Here, E^- and C are denoted as the lower bounds of the longitudinal modulus and volume fraction of inclusion, respectively. Also, p and i subscripts are the indicated polymer and inclusion. The upper bounds can be calculated by subjecting the basic uniaxial test specimen to elongation and estimating the associated strain energy U*. The actual strain energy is U. The inequality is U < U* and the equation will be,

$$E_c^+ \leq \frac{1-V_i-4V_iV+2V^2}{1-V_i-2V_i^2}E_iC + \frac{1-V_p-4V_pV+2V^2}{1-V_p-2V_p^2}E_p(1-C) \tag{2}$$

where, E^+ = upper bounds of the longitudinal modulus, ν = Poisson's ratio.

$$V = \frac{\left(1-V_p-2V_p^2\right)V_iE_iC + \left(1-V_i-2V_i^2\right)V_pE_p(1-C)}{\left(1-V_p-2V_p^2\right)E_iC + \left(1-V_i-2V_i^2\right)E_p(1-C)} \tag{3}$$

Now both lower and upper bounds of the composites' modulus can be calculated and compared with the experimental values.

3.2. Prediction of Strength (Shear Lag Model)

When the particles are fiber-like CNTs and these are aligned in a particular direction inside the polymer then the load transfer to the reinforcing particles and the composite strength can be calculated by a micromechanics-based shear lag model. For this model, the governing differential equation for stress distribution in the fiber is [30–32]:

$$\frac{d^2\sigma_{f=}}{dx^2} = \frac{n^2}{r^2}\left(\sigma_f - E_f\,\varepsilon_1\right) \tag{4}$$

Here, x = distance from the mid-point of the fiber, r = radius of the fiber/tube, ε = composite strain and n = dimension less constant given by: $a^{1/2}$

$$n = \left[\frac{2E_m}{E_f\,(1-V_m)\ln\left(\frac{1}{c}\right)}\right]^{1/2} \tag{5}$$

m and f subscripts denote the matrix polymer and inclusion, respectively. The above 2nd order differential equation can be solved as,

$$\sigma_{f=}\,E_f\,\varepsilon_1 + B\,\sin\,h\left(\frac{nx}{r}\right) + D\,\cos\,h\left(\frac{nx}{r}\right)\,] \tag{6}$$

Considering $x = \pm$ L, where L = fiber half-length, and fiber aspect ratios = L/r,

$$\sigma_{f=}\,E_f\,\varepsilon_1\,[1-\cosh\left(\frac{nx}{r}\right)\sec\,h(ns)\,] \tag{7}$$

The strength of the composite can now be determined from the rule of mixture as:

$$\sigma_c = (1-c)\sigma_{matrix} + c\sigma_f \tag{8}$$

where, σ_{matrix} is the average matrix strength.

The average reinforcing fiber stress (integration of Equation (7)) is

$$\overline{\sigma_f} = \varepsilon_1 E_f[1-\frac{\tanh(ns)}{ns}] \tag{9}$$

4. Results and Discussion

4.1. Tensile Testing

Five categories of materials, namely, neat CA and CA-MWCNT with 0.5%, 1.0%, 1.5%, 2.0% reinforced samples, were tested under tension. The standard deviation was determined and an average value of 4 data sets was taken to get more accurate data. There were 3 or more random samples in each set. The representative stress-strain curves for neat and nanocomposite specimens are shown in Figure 4 and tensile data in tabular form is shown in Table 1. It was observed that the tensile strength was increased by adding a CNT percentage with CA up to 1.5%. Without CNT, the tensile strength was 59 MPa. After adding 0.5% to 1.5 wt. % CNT the tensile strength was 97.50 MPa, but with a further increase of CNT loading of 2 wt. % the strength decreased to 63.25 MPa. The same trend was observed in the modulus, ultimate strength, fracture strain, and toughness.

The Young's modulus was higher with 1.5 wt. % CNT loaded fiber. Ultimate tensile strength was almost double in 1.5 wt. % CNT-reinforced fiber. Increase in the modulus can be attributed to the

infusion of much stiffer CNT in CA according to the rule of mixture. The enhancement of yield strength (0.2% offset) was 79% for 1.5 wt. % CNT loaded fiber. Increase in strength suggests the presence of a strong attraction between the polymer and the nanotubes, and load transfer to the reinforcing particles. When the reinforcement loading reaches 2 wt. %, it may reach its perturbation and thus shows a decrease in strength and modulus.

The trapezoidal rule was used to measure the area under the stress-strain curves shown in Figure 4. This area under the curve is the indicator of the fibers' modulus of toughness. An increase in the modulus of toughness by 25 MPa was observed in 1.5 wt. % MWCNT-reinforced samples. The average modulus of toughness was decreased by 9 MPa for 1.5–2.0 wt. % CNT loaded fibers. The CNT loaded fiber was able to absorb more energy than neat CA fiber. Fracture strain was increased by adding MWCNT to CA fiber.

Due to variation in the standard deviation, an analysis of variance (ANOVA) test was done to reject the null hypothesis that all groups of fiber have equal properties despite different MWCNT loading following the approach mentioned by Fisher [33]. From the ANOVA calculation done on the data set, it is seen that the ratio between mean square variations between different groups to mean square variation within each group is 7.8977, which is commonly known as the F value. Since the observed F value is more than the critical F value of 3.804, the null hypothesis can be rejected. Measured p-value is found to be 0.001238 which is less than the significance value of 0.05 considered in this calculation. The p and F values, reject the null hypothesis and accept the alternate hypothesis that the loading of MWCNT affects the mechanical properties of CA fiber.

It is noteworthy that above a 1.5 wt. % concentration of MWCNT in the CA polymer matrix solution, the flow viscosity of the solution increased to a level where continuous production of filaments was very difficult and a higher shear force was necessary to drag the polymer solution for fiber processing. In this process, polymer chain cession is more likely to happen which we observed through the breakdown of the filaments. However, with a loading percentage of <2%, we did not observe any significant fiber breakdown during the processing and improved mechanical properties. Amongst all the loadings, a 0.5% loading has the minimal impact on the mechanical properties. Similar phenomenon have been observed during CNT inclusion in polyethylene-based polymer systems [34,35] where 2 wt. % of CNT loading was found to be effective. In addition, some other previous studies [32,36] using reinforcement of nanotubes or nanoparticles in thermoplastic polymer system, also suggest that concentrations of CNTs usually vary between 0–2 wt. %.

4.2. Theoretical Prediction of Modulus and Strength

To predict the modulus and shear strength of MWCNT-reinforced CA, the property values for the polymer matrix and the inclusion was used from Table 2.

For the theoretical modulus calculation, Poisson's ratio corresponding to minimum strain energy was calculated from Equation (3) and used in Equation (2) to calculate the upper modulus. The lower modulus is calculated from Equation (1) and it is found to be more or less similar for all the percentages of inclusion which are listed in Table 3. The upper modulus increases significantly with the increased inclusion percentage. The upper bounds of the longitudinal modulus increased from 5.5 GPa to 14.7 GPa when the inclusion was increased from 0.5% to 2.0%. This increase of modulus is predictable with the rule of mixture. However, the experimental results showed the increasing trend of the modulus only up to 1.5% and after that it decreased as can be seen in Table 1.

The range of composite strength can be calculated from Equation (8), as the interfacial shear stress varies along the length of the acicular CNT reinforcement. The yield strength of the neat CA fiber was used as the matrix value. ε_1 = approximate strain in the composites up to the proportional limit, r = radius of the nanotube = 15 nm for MWCNT, s = L/r =7.5 μ/15 nm = 500 for MWCNT. Composites strengths were computed with various values of x from the mid-point to the tip of the MWCNT from Equation (7) which can be seen in Table 4 which shows the calculated values of average composite strength for different percentages of MWCNT inclusion in CA composite fiber. It is

observed in Table 5 that the calculated strength increased with the increased percentage of inclusion, however, experimental strength only increased up to 1.5% of CNT inclusion and decreased at 2.0% of CNT loading.

Table 2. Property values for matrix and inclusion.

Parameters	Cellulose Acetate	Multi-Walled Carbon Nanotubes
Loading (wt %)	-	0.5–2%
Young's Modulus (GPa)	2.4	1000
Modulus of Rigidity (GPa)	0.8628	469
Poisson's Ratio	0.38	0.28
Density (gm/cm^3)	1.28	2.1

Table 3. Calculated and experimental values of modulus.

CNT Loading%	Reinforcement Volume Fraction (C)	Composite Poisson's Ration: v	Calculated Lower Modulus Ep^- (GPa)	Calculated Upper Modulus Ep^+ (GPa)	Experimentally Measured E_{11} (GPa)
0.5	0.0030	0.3372	2.407	5.428	1.79
1.0	0.0061	0.3201	2.415	8.5301	1.81
1.5	0.0091	0.3109	2.422	11.5376	1.97
2.0	0.0120	0.3051	2.430	14.5220	1.56

Table 4. Calculated strength over the MWCNT length for different inclusion percentages.

X (μm)	Composite Strength, σ_c for 0.5% Inclusion (MPa)	Composite Strength, σ_c for 1.0% Inclusion (MPa)	Composite Strength, σ_c for 1.5% Inclusion (MPa)	Composite Strength, σ_c for 2.0% Inclusion (MPa)
0	59.0	59.0	59.0	59.0
2.5	253.58	419.65	555.93	662.16
5.0	256.86	424.29	561.26	667.75
7.5	256.91	424.35	561.32	667.80
10	256.86	424.29	561.26	667.75
12.5	253.58	419.65	555.93	662.16
15	59.0	59.0	59.0	59.0

Table 5. Calculated and experimental strength of CA-MWCNT.

Inclusion Percentage %	Average Composite Strength, σ_c Based on Shear Lag Model (MPa)	Experimental Yield Strength σ_c (MPa)
0.5	240.75	79.25
1.0	424.49	82.25
1.5	609.08	97.50
2.0	794.25	63.25

5. Characterization

5.1. Scanning Electron Microscope

The cross section of neat CA fiber showed a 0.25 μm tiny void surface (Figure 5a). However, the CA-MWCNT fiber section showed irregular features and 0.5 μm voids (Figure 5b), which is almost double the size of neat CA. The TGA (Thermogravimetric analysis) study showed the lower water retention of CA-MWCNT fiber than neat CA [37]. This result suggests that the lower water retention is causing the micro voids in the composite fiber. During post-processing of fiber, vacuuming, and heating for 2 h, the water was removed. We believe more water removal happened in CNT loaded

fiber than pure fiber. Therefore, the void diameter of CNT loaded fiber was larger than neat fiber. In Figure 5b, an SEM image of CA-MWCNT fiber, the diameter of the voids was measured and these varied from 0.4 to 0.6 μm.

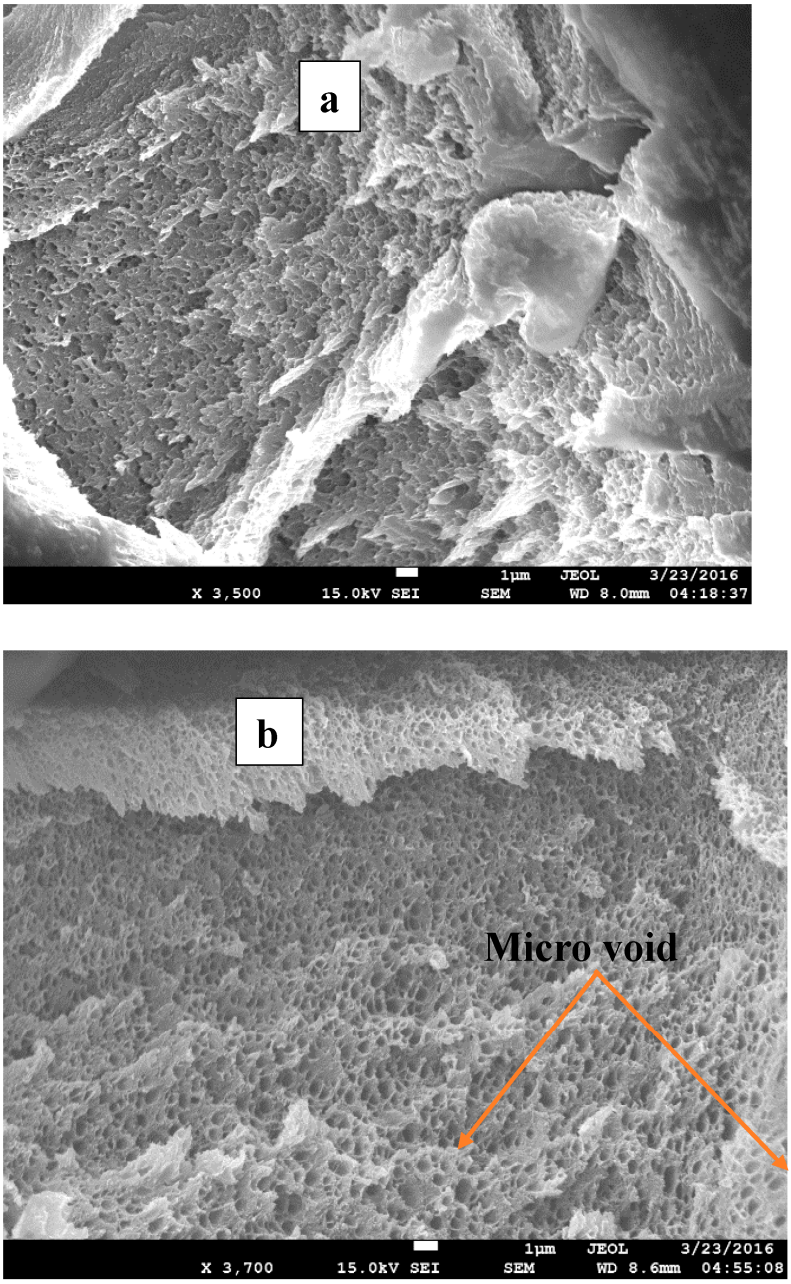

Figure 5. SEM image of a cross section of (**a**) neat CA fiber (**b**) CA-MWCNT 0.5 wt. % fiber.

A longitudinal view of both neat CA (Figure 6a) and CA-MWCNT (Figure 6b) from the SEM image shows surface texture. Figure 6a shows crazes on some parts of the surface and a smooth surface at other points. Also, Figure 6b shows a smooth surface. Post-processing of the fiber helps to improve fiber defects. Stretching can decrease the crazes on the surface and voids on the cross section of the diameter.

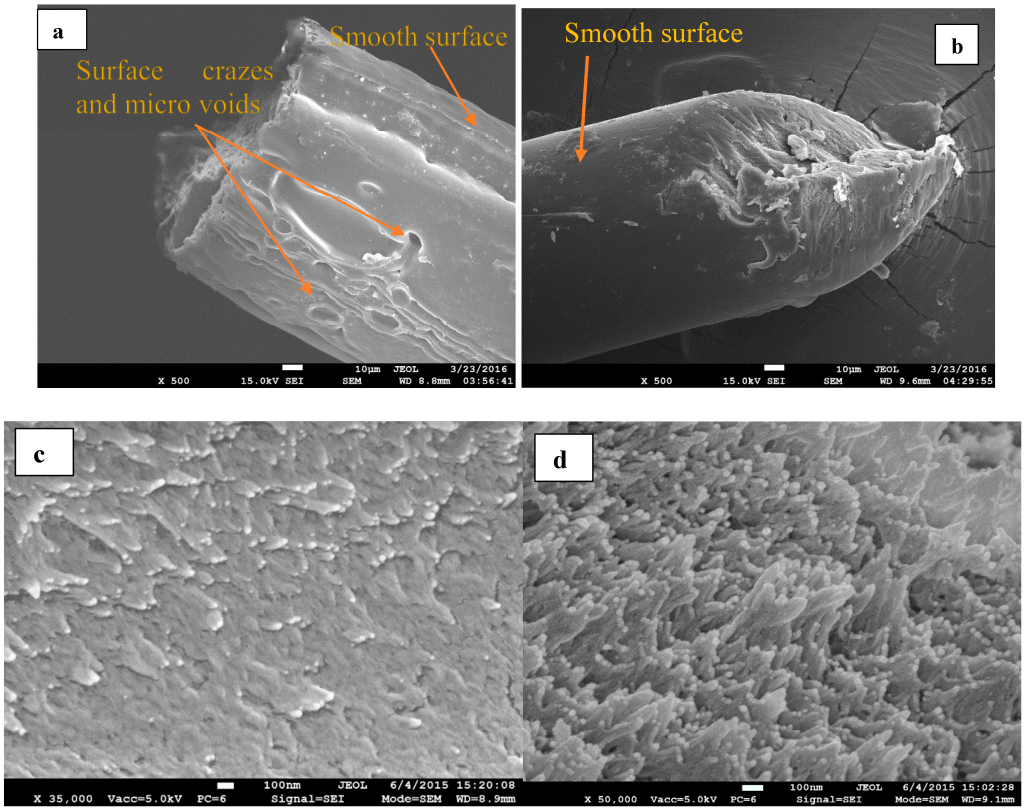

Figure 6. SEM image of (**a**) longitudinal outer surface of neat CA fiber (**b**) longitudinal outer surface of CA-MWCNT 0.5 wt. % fiber (**c**) cross-sectional view of neat CA fiber (**d**) cross-sectional view of CA-MWCNT 0.5 wt. % fiber.

In Figure 6c,d, cross-sectional views of CNT loaded CA fiber show a higher degree of nanofibrillar structure than neat CA. The surface area of cellulose is expanded by interconnected fibrils. For this reason, nanofibrillar cellulose is produced; and also high strength and high modulus is achieved. It was observed from the SEM images that both the fibrillation and the porosity (as shown in Figure 6) were increased with the inclusion of CNT in the fiber. It has been observed previously that the average strength and modulus increases with the increase of porosity from 19% to 40%, and the high toughness of highly porous cellulose nanopapers is related to nanofibrillar network structure [38]. In our previous work [39], less presence of water was detected on CA-CNT samples compared to control samples. As can be observed from the SEM pictures (Figure 6) the enhanced interconnected nanofibrillation in the CNT-reinforced CA samples resulted in improved mechanical properties. We believe, the nanotubes' surface energy has incorporated a more favorable site for matrix polymer nucleation and fibrillation. In Figure 7, the energy-dispersive X-ray spectroscopy (EDS) study showed that neat CA fiber has 57.5 wt. % of C, and after the addition of MWCNT the percentage increased to 60.3%. The carbon molecule count was increased from 5400 to 6200 on the cross section of the fiber. The percentage of O was decreased about 3% but the oxygen count was unchanged (3000), which indicated the inclusion of CNT into the polymer matrix.

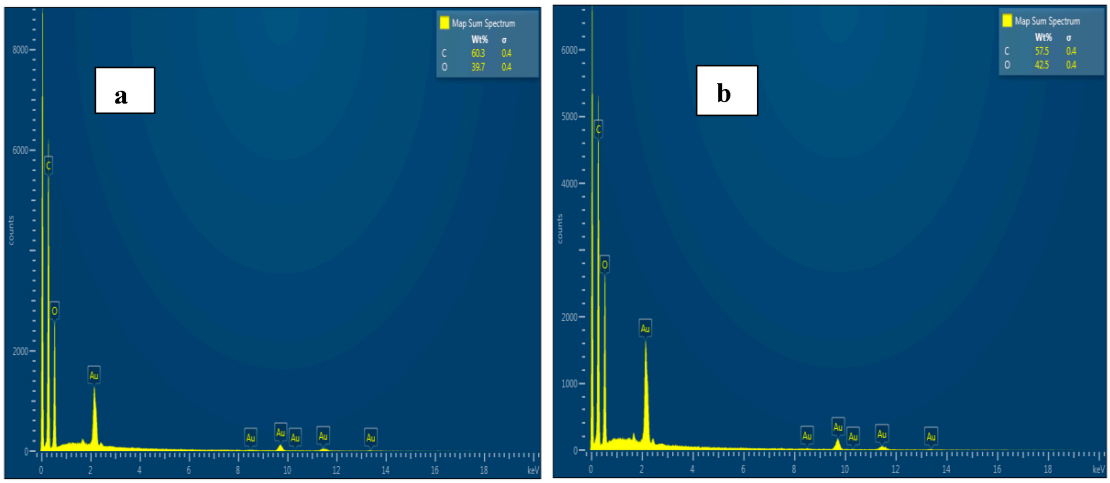

Figure 7. EDS plot of a cross section of (**a**) neat CA fiber (**b**) CA-MWCNT fiber 0.5 wt. % fiber.

5.2. Fourier Transform Infrared Spectroscopy (FTIR) Analysis

The absorption peaks in the IR spectrum of 1743, 1368 and 1238 cm^{-1} correspond to C=O ester stretching group, C–H group and C-O group, respectively. The FTIR spectra in Figure 8 shows no significant shift of wavenumber for the inclusion of MWCNT in the CA matrix, which indicates that the sonication process of CNT-loaded solution did not degrade the CA bonding structure. MWCNTs show the characteristic G (1593 cm^{-1}) and D (1350 cm^{-1}) in Figure 8.

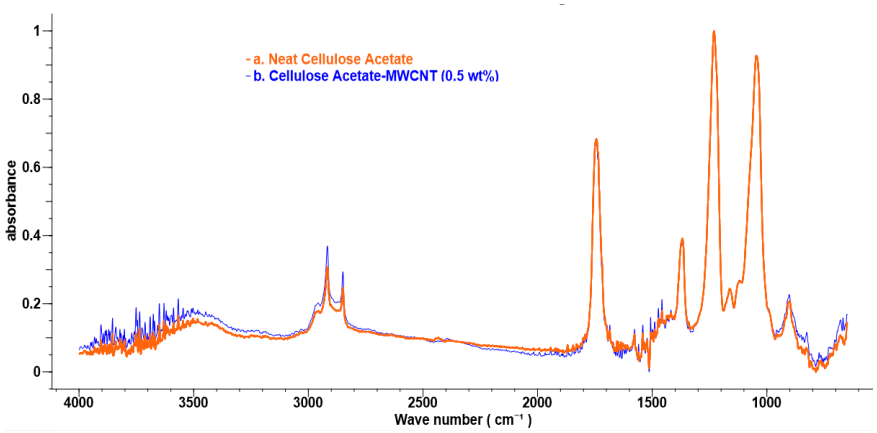

Figure 8. FTIR absorbance spectra of (**a**) neat CA (**b**) CA-MWCNT.

Table 6 shows the area for bending. Wagging and rocking modes decreased after the addition of CNT in the polymer, but the stretching mode was increased for C–H and C=O bonds. Absorbance peaks at ~2360 cm^{-1} suggest the presence of an O=C=O asymmetric stretch [40]. The absorbance peak at 2360 cm^{-1} was flattened by the KnowItAll IR spectral analysis software. The presence of O=C=O absorbance peaks suggests possible thermo-oxidative degradation of blends during processing. McKittrick et al. [41] have shown that characteristic IR bands of imides consist of carbonyl groups around 1750–1700 cm^{-1} and a C–N–C stretching band around 1210–1140 cm^{-1}. In Table 6, wavenumbers, 1161 and 1158 cm^{-1} indicate the presence of the residual solvent (DM) in the fiber matrix. The characteristic bands of CA in the IR spectrum were observed in curve 8(a). A broad absorption band at 2700–2900 cm−1 is attributed to $–CH_2$ groups (CH stretching) [42,43] .

Table 6. Characteristic FTIR absorbance peaks.

	Wavenumber (cm^{-1})		Area		
Bonding	CA	CA-MWCNT	CA	CA-MWCNT	
C–H Bending	900	902	5.70	4.06	A_1
C–O Stretching/C–H Bending	1046	1046	25.07	12.30	A_2
C–H Wag	1161	1158			
C–O Stretching/C–H Wag	1230	1231	20.08	9.90	A_3
C–H Rock	1368	1368	7.70	3.30	A_4
C=O Stretching	1743	1743	6.59	10.82	A_5
C–H Stretching	2849	2849			
C–H Stretching	2917	2916	4.77	8.34	A_6

The wavenumbers, 1046, 1230 cm^{-1} indicated an acetyl group and 1743 cm^{-1} indicated an C=O ester stretching group. A significant decrease in area (A_1, A_2, A_3, A_4) was found for C–H bending, wagging and rocking. However, the area A_5 was increased for bonding of C–H stretching from 4.77 to 8.34, and A_6 was also increased for C=O stretching from 6.59 to 10.82.

Also, for the combination of CNT with CA, the methylene C–H deformation peaks were shifted slightly to lower wavenumbers from 1161 to 1158 cm^{-1} for wagging and 2917 to 2916 cm^{-1} for stretching and the bending C–H bonding was increased from 900 to 902 cm^{-1}.

6. Conclusions

Neat CA and (0.5–2.0 wt. %) MWCNT loaded CA composite fibers were produced by a solution spinning process. From the tensile testing of the produced fibers, it was observed that yield strength, modulus, ultimate tensile strength, fracture strain and toughness increased by inclusion of MWCNT with CA, up to 1.5 wt. %, but with the further inclusion of MWCNTs in CA the values decreased.

The SEM study showed that the void diameter of CNT loaded fiber was larger than neat fiber, which is almost double the size of neat CA. Due to the lesser water retention capability of MWCNT-reinforced CA, more water removal happened in CNT loaded fiber than in pure fiber. Few crazes are found on the surface of the fiber. The porous fibrils of CNT loaded fiber showed higher mechanical strength and toughness than neat fiber. EDS study showed that neat CA fiber has 57.5 wt. % of C and after addition of MWCNT the percentage increased to 60.3%, which indicated the inclusion of CNT into the polymer matrix.

FTIR tests revealed that the area for bending, wagging, and rocking modes were decreased after the addition of CNT in the polymer, but the stretching mode was increased for C–H and C=O bonds. By including CNT with CA, the methylene C–H deformation peaks were shifted slightly to lower wavenumbers, from 1161 to 1158 cm^{-1} for wagging and 2917 to 2916 cm^{-1} for stretching, and the bending C–H bonding was increased from 900 to 902 cm^{-1}.

Acknowledgments: The authors would like to acknowledge support from the Mechanical Engineering department of Georgia Southern University and are grateful to Hao Chen for assisting with the SEM imaging. The authors would also like to thank Rafael Quirino and Nathan Takas for helping with FTIR tests.

Author Contributions: Mujibur Khan and Quazi Nahida Sultana conceived and designed the experiments; Quazi Nahida Sultana and Sakib Iqbal performed the experiments; Mujibur Khan and Aniruddha Mitra analyzed the data; Mujibur Khan, Md Mahmudul Hassan and Ishraq Shabib contributed reagents/materials/analysis tools; Quazi Nahida Sultana and Md Mahmudul Hassan wrote the paper.

Conflicts of Interest: The authors declare no conflict of interest.

References

1. Tan, S.S.Y.; MacFarlane, D.R. *Ionic Liquids*; Springer: Berlin, Germany, 2009; pp. 311–339.
2. Kim, I.S.; Kim, J.P.; Kwak, S.Y. Novel Regenerated Cellulosic Material Prepared by an Environmentally-Friendly Process. *Polymer* **2006**, *47*, 1333–1339. [CrossRef]

3. Serad, G.A. Fibers, Cellulose Esters. In *Kirk-Othmer Encyclopedia of Chemical Technology*; John Wiley & Sons, Inc.: New York, NY, USA, 2000. [CrossRef]
4. Dos Santos Rosa, D.; Lenz, D.M. Biocomposites: Influence of Matrix Nature and Additives on the Properties and Biodegradation Behaviour. In *Biodegradation–Engineering and Technology*; InTech: Rijeka, Croatia, 2013; pp. 433–475.
5. Harnnecker, F.; dos Santos Rosa, D.; Lenz, D.M. Biodegradable Polyester-Based Blend Reinforced with Curau Fiber: Thermal, Mechanical and Biodegradation Behaviour. *J. Polym. Environ.* **2012**, *20*, 237–244. [CrossRef]
6. Eichhorn, S.J.; Dufresne, A.; Aranguren, M. Review: Current International Research into Cellulose Nanofibres and Nanocomposites. *J. Mater. Sci.* **2010**, *45*, 1–33. [CrossRef]
7. Tungprapa, S.; Puangparn, T.; Weerasombut, M. Electrospun Cellulose Acetate Fibers: Effect of Solvent System on Morphology and Fiber Diameter. *Cellulose* **2007**, *14*, 563–575. [CrossRef]
8. Pillay, V.; Dott, C.; Choonara, Y.E. A Review of the Effect of Processing Variables on the Fabrication of Electrospun Nanofibers for Drug Delivery Applications. *J. Nanomater.* **2013**, *2013*, 789289. [CrossRef]
9. Ach, A. Biodegradable Plastics Based on Cellulose Acetate. *J. Macromol. Sci. Part A* **1993**, *30*, 733–740. [CrossRef]
10. Yu, M.; Lourie, O.; Dyer, M.J. Strength and Breaking Mechanism of Multiwalled Carbon Nanotubes under Tensile Load. *Science* **2000**, *287*, 637–640. [CrossRef] [PubMed]
11. Wilder, J.W.; Venema, L.C.; Rinzler, A.G. Electronic Structure of Atomically Resolved Carbon Nanotubes. *Nature* **1998**, *391*, 59–62. [CrossRef]
12. Arash, B.; Wang, Q. Detection of Gas Atoms with Carbon Nanotubes. *Sci. Rep.* **2013**, *3*, 1782. [CrossRef]
13. Wang, Q. Atomic Transportation via Carbon Nanotubes. *Nano Lett.* **2008**, *9*, 245–249. [CrossRef] [PubMed]
14. Lau, K.; Gu, C.; Hui, D. A Critical Review on Nanotube and Nanotube/Nanoclay Related Polymer Composite Materials. *Compos. Part B* **2006**, *37*, 425–436. [CrossRef]
15. Coleman, J.N.; Khan, U.; Blau, W.J. Small but Strong: A Review of the Mechanical Properties of Carbon Nanotube–polymer Composites. *Carbon* **2006**, *44*, 1624–1652. [CrossRef]
16. Ajayan, P.M.; Stephan, O.; Colliex, C. Aligned Carbon Nanotube Arrays Formed by Cutting a Polymer Resin–nanotube Composite. *Science* **1994**, *265*, 1212–1214. [CrossRef] [PubMed]
17. Garg, A.; Sinnott, S.B. Effect of Chemical Functionalization on the Mechanical Properties of Carbon Nanotubes. *Chem. Phys. Lett.* **1998**, *295*, 273–278. [CrossRef]
18. Ajayan, P.M.; Schadler, L.S.; Giannaris, C. Single-Walled Carbon Nanotube–polymer Composites: Strength and Weakness. *Adv. Mater.* **2000**, *12*, 750–753. [CrossRef]
19. Ni, B.; Sinnott, S.B. Chemical Functionalization of Carbon Nanotubes through Energetic Radical Collisions. *Phys. Rev. B* **2000**, *61*, R16343. [CrossRef]
20. Treacy, M.J.; Ebbesen, T.W.; Gibson, J.M. Exceptionally High Young's Modulus Observed for Individual Carbon Nanotubes. *Nature* **1996**, *381*, 678–680. [CrossRef]
21. Lourie, O.; Cox, D.M.; Wagner, H.D. Buckling and Collapse of Embedded Carbon Nanotubes. *Phys. Rev. Lett.* **1998**, *81*, 1638. [CrossRef]
22. Lourie, O.; Wagner, H.D. Evaluation of Young's Modulus of Carbon Nanotubes by Micro-Raman Spectroscopy. *J. Mater. Res.* **1998**, *13*, 2418–2422. [CrossRef]
23. Thostenson, E.T.; Chou, T.W. Aligned multi-walled carbon nanotube-reinforced composites: Processing and mechanical characterization. *J. Phys. D Phys.* **2002**, *35*, L77. [CrossRef]
24. Bhattacharyya, A.; Joshi, M. Nanotechnology—A New Route to High-Performance Functional Textiles. *Text. Prog.* **2011**, *43*, 155–233.
25. Gupta, M.; Lin, Y.; Deans, T. Biaxially Oriented Poly (Propylene-G-Maleic Anhydride)/Phosphate Glass Composite Films for High Gas Barrier Applications. *Polymer* **2009**, *50*, 598–604. [CrossRef]
26. Gupta, M.; Lin, Y.; Deans, T. Structure and Gas Barrier Properties of Poly (Propylene-Graft-Maleic Anhydride)/Phosphate Glass Composites Prepared by Microlayer Coextrusion. *Macromolecules* **2010**, *43*, 4230–4239. [CrossRef]
27. Greco, A.; Ferrari, F.L.; Mafezzoli, A. Processing and characterization of amorphous plyethylene terephthalate fibers for the alignment of carbon nanofillers in thermosetting resins. *Polym. Compos.* **2015**, *36*, 1096–1103. [CrossRef]
28. Ponnie, R.; Kontturi, E.; Vourinen, T. Accessibility of celloluse: Straictural changes and their reversibiliy in aqueous media. *Carbohydr. Polym.* **2013**, *93*, 424–429. [CrossRef] [PubMed]

29. Jones, R. *Mechanics of Composites Materials*, 2nd ed.; Hemisphere Publishing Corporation: New York, NY, USA, 1998.
30. Hull, D.; Clyne, T.W. *An Introduction to Composite Materials*; Cambridge University Press: New York, NY, USA, 1996.
31. Cox, H.L. The Elasticity and Strength of Paper and Other Fibrous Materials. *Br. J. Appl. Phys.* **1952**, *3*, 72. [CrossRef]
32. Mahfuz, H.; Adnan, A.; Rangari, V.K. Enhancement of Strength and Stiffness of Nylon 6 Filaments through Carbon Nanotubes Reinforcement. *Appl. Phys. Lett.* **2006**, *88*, 083119. [CrossRef]
33. McDonald, J.H. *Handbook of Biological Statistics*, 3rd ed.; Sparky House Publishing: Baltimore, MD, USA, 2014.
34. Mahfuz, H.; Khan, M.R.; Leventouri, T. Investigation of MWCNT Reinforcement on the Strain Hardening Behavior of Ultrahigh Molecular Weight Polyethylene. *J. Nanotechnol.* **2011**, *2011*, 637395. [CrossRef]
35. Khan, M.R.; Mahfuz, H.; Leventouri, T. Enhancing Toughness of Low-density Polyethylene Filaments through Infusion of Multiwalled Carbon Nanotubes and Ultrahigh Molecular Weight Polyethylene. *Polym. Eng. Sci.* **2011**, *51*, 654–662. [CrossRef]
36. Mahfuz, H.; Adnan, A.; Rangari, V.K. Manufacturing and Characterization of Carbon Nanotube/Polyethylene Composites. *Int. J. Nanosci.* **2005**, *4*, 55–72. [CrossRef]
37. Mahfuz, H.; Hasan, M.M.; Rangari, V.K. Reinforcement of Nylon-6 Filaments with SiO_2 Nanoparticles and Comparison of Young's Modulus with Theoretical Bounds. *Macromol. Mater. Eng.* **2007**, *292*, 437–444. [CrossRef]
38. Marielle, H.; Lars, A.B.; Per, I.; Tom, L.; Takashi, N. Cellulose Nanopaper Structures of high Toughness. *Biomacromolecules* **2008**, *9*, 1579–1585.
39. Sultana, Q.N.; Absar, S.; Hulsey, S. Synthesis and Processing of Solution Spun Cellulose Acetate Fibers Reinforced With Carbon Nanotubes. In Proceedings of the ASME 2015 International Mechanical Engineering Congress & Exposition, Houston, TX, USA, 13–19 November 2015; IMECE2015-50804, p. V009T12A070.
40. Larkin, P. *Infrared and Raman Spectroscopy; Principles and Spectral Interpretation*; Elsevier: Waltham, MA, USA, 2011; ISBN 9780123870186.
41. Utracki, L.A. Fibers from Polymeric Nanocomposites. *Indian J. Fibre Text. Res.* **2006**, *31*, 15–28.
42. McKittrick, P.T.; Katon, J.E. Infrared and Raman Group Frequencies of Cyclic Imides. *Appl. Spectrosc.* **1990**, *44*, 812–817. [CrossRef]
43. Pielesz, A.; Biniaś, W. Cellulose Acetate Membrane Electrophoresis and FTIR Spectroscopy as Methods of Identifying a Fucoidan in Fucusvesiculosus Linnaeus. *Carbohydr. Res.* **2010**, *345*, 2676–2682. [CrossRef] [PubMed]